Pipe flow of a dense emulsion: homogeneous shear-thinning or shear-induced migration ?

Micheline Abbas, Amélie Pouplin, Olivier Masbernat, Alain Liné, Sandrine Decarre

Pipe Flow of a Dense Emulsion: Homogeneous Shear-Thinning or Shear-Induced Migration?

Micheline Abbas
Laboratoire de Génie Chimique, Université de Toulouse, CNRS-INPT-UPS, Toulouse, France

Fédération de recherche FERMaT FR CNRS 3089, Toulouse, France

Amélie Pouplin
Dept. de Mécanique Appliquée, IFP, Rueil-Malmaison, France

Laboratoire de Génie Chimique, Université de Toulouse, CNRS-INPT-UPS, Toulouse, France

Fédération de recherche FERMaT FR CNRS 3089, Toulouse, France

Olivier Masbernat
Laboratoire de Génie Chimique, Université de Toulouse, CNRS-INPT-UPS, Toulouse, France

Fédération de recherche FERMaT FR CNRS 3089, Toulouse, France

Alain Liné
Laboratoire d'Ingénierie des Systèmes Biologiques et des Procédés, Université de Toulouse, INSA, Toulouse, France

Fédération de recherche FERMaT FR CNRS 3089, Toulouse, France

Sandrine Décarre
Dept. de Mécanique Appliquée, IFP, Rueil-Malmaison, France

DOI 10.1002/aic.15811

The flow field of a 70% concentrated noncolloidal o/w emulsion in a pipe has been investigated by means of Particle Image Velocimetry in a matched refractive index medium. At steady state and in laminar regime, the shape of axial velocity profiles is not parabolic and exhibits a shear-thinning behavior of the dense emulsion, with a flow index of 0.5 and a negligible yield stress (less than 1 Pa). However, instead of a square root law, the pressure drop increases linearly with U_m. To explain this apparent inconsistency, two mechanisms of different nature are considered. The first originates from a possible relation between the consistency factor and the drop mean diameter. The second mechanism is shear-induced migration and leads to the development of a concentration gradient in the pipe cross section. Both mechanisms considered reconcile the experimental data, the apparent local shear-thinning behavior and the linear evolution of the pressure drop with the flow rate. *AIChE J*, 63: 5182–5195, 2017
*Keywords: emulsion, rheology, p*ipe flow*,* shear thinning*,* shear-*induced migration*

Introduction

Optimization and/or scaling-up of processes involving concentrated noncolloidal emulsions require adequate models for the transport of these emulsions, and until now this issue has motivated a large number of works devoted to the modeling of transport properties of emulsions (shear viscosity, normal stresses, diffusivity, and viscoelastic moduli), based on theoretical, experimental and numerical rheological studies, starting with the early works of Einstein and Taylor. Compared to the case of suspensions, emulsions increase the level of complexity, due to the deformability, the control of boundary conditions at the oil/water interface (due to the presence of contaminant or surfactants), and of the polydispersity. These three parameters greatly influence the dynamic response of an emulsion to a stress, and as a result, the development of rheological models for concentrated emulsions is still mainly based on experimental studies in simple flow geometries (cf. for instance, Derkach,[1] Datta et al.,[2] and Cohen-Addad and Höhler[3]). However, there are little data on the validation of these rheological models for concentrated emulsions in real flow conditions of Blondin and Doubliez,[4] Meeker et al.,[5] and

Correspondence concerning this article should be addressed to O. Masbernat at olivier.masbernat@ensiacet.fr

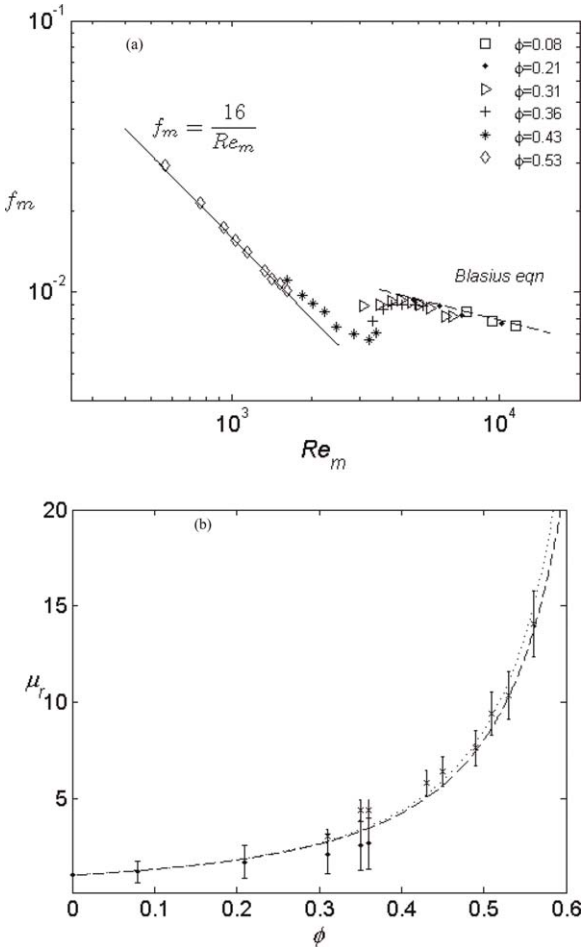

Figure 1. (a) Wall friction factor as a function of the mixture Reynolds number at various concentrations ($\mathrm{Re}_m = \rho_m U_m D/\mu_m$) from Pouplin et al.[6]; (b) relative viscosity as a function of oil volume fraction ($\phi_M = 0.74$).

(. . .) Eilers; (– –) Krieger and Dougherty; (◆) Blasius friction factor; (×) Hagen–Poiseuille friction factor.

Pouplin et al.,[6] and this is mainly due to the difficulty of implementing at a local-scale noninvasive measurement techniques in such flows.[7] The question of representativeness of rheological laws for real flows therefore arises, in particular when the shear rate field is not homogeneous such as in a pipe flow.[8,9]

In a previous work, the local structure of a homogeneous pipe flow of a noncolloidal oil-in-water emulsion has been investigated in Pouplin et al.[6] for a wide range of concentration (from dilute to 56%) and flow regimes (laminar, turbulent, and intermittent). This work has clearly demonstrated the relevance of the concept of effective medium (mixture viscosity) for emulsions in fully developed laminar and turbulent regimes (cf. Figures 1a, b). The shear viscosity is well described by an Eilers' or Krieger and Dougherthy's law up to a volume fraction ϕ equal to 0.6, taking a maximum packing fraction $\phi_M = 0.74$

$$\mu_r = (1-\phi/\phi_M)^{-2.5\phi_M} \quad (1)$$

Note that the model of Choi and Showalter[10] reasonably well reproduces the experimental trend up to $\phi = 0.55$, but with a viscosity ratio λ 4 times larger than its real value. A similar trend is observed with the model proposed by Pal,[11] which underestimates the evolution of the relative viscosity with volume fraction of the present system (agreement is obtained with a viscosity ratio equal to 8 instead of the current value $\lambda = 0.125$). The model of Yaron and Gal-Or[12] widely underestimates the data over the whole range of concentration, assuming mobile ($\lambda = \mu_d/\mu_c$) or immobile ($\lambda \to \infty$) interfaces.

In transient regime,[13] the macroscopic behavior is however modified compared to a single Newtonian fluid and cannot be solely described by a Reynolds number based upon mixture viscosity and density, as previously observed by Matas et al.[14] in horizontal flows of neutrally buoyant suspensions.

For larger drop volume fractions, the increase of the apparent viscosity is accompanied with the emergence of a strong non-Newtonian behavior, the transition occurring in the range of concentration 60%–70%.[15] Various non-Newtonian behaviors were reported in the literature that can be described by macroscopic shear thinning or viscoelastic laws.[16–18] The non-Newtonian behavior is often attributed to polydispersity and/or drop deformation.[19] Note also that deviation from an effective fluid behavior of the emulsion was observed in microchannels by Goyon et al.,[20] induced by finite drop size effects or rough channel walls (nonlocal effects).

When the material is homogeneous, local constitutive laws can be directly inferred from macroscopic rheological measurements. This fact has been evidenced by local velocity measurements in nonadhesive concentrated emulsion flows in a wide-gap Couette apparatus,[16] where a Herschel–Bulkley model (shear-thinning with a yield stress) was found to fully describe the local and macroscopic rheology of the homogeneous emulsion. However, the rheology of dense flows is not always perfectly concordant at all length scales. For example, in Couette flow laden with rigid particles at high solid volume fraction, Ovarlez et al.[21] showed that constitutive laws derived from local velocity profile measurements disagree with that deduced from the torque-rotation speed relation in the device. They obtained a factor 5 (at 60% volume fraction) between viscosities calculated at the local and rheometer scales. The discrepancy was ascribed to the establishment of a concentration profile resulting from particle migration toward the outer cylinder where the shear rate is the lowest.

In the present work, we have extended the pipe flow investigations presented in Pouplin et al.[6] to the case of a highly concentrated emulsion below the glassy transition (volume fraction of 0.7) of noncolloidal (20 μm diameter) oil drops in an aqueous phase, where shear-thinning behavior is usually observed. Objectives are to test at a local scale in a nonuniform flow the relevance of the concept of effective medium in this range of concentration. In particular, the local flow rheology is investigated at different mixture velocities in the pipe cross section and its consistency with the macroscopic momentum balance is discussed.

The article is structured as follows: in the second section a short description of the experimental setup and measurement techniques are presented as well as the flow parameters. Matching the refractive index of the two phases, the velocity field in a 5-cm diameter pipe could be accurately measured at different mixture velocities in laminar regime using Particle Image Velocimetry (PIV) technique. For a steady, established, and parallel emulsion flow with drop concentration homogeneously distributed over the pipe cross section, the measurement of the velocity profile in the cross section provided a stress–strain relation at a local scale. For each flow rate, the

Table 1. Physical Properties of Liquid Phases at 29°C

Phases		ρ (kg m^{-3})	μ (Pa s)	n_D	σ (N m^{-1})
Dispersed	n-heptane	$\rho_d = 684$	$\mu_d = 4 \times 10^{-4}$	1.385	0.031
Continuous	water–glycerin (43% vol)	$\rho_c = 1102$	$\mu_c = 3.2 \times 10^{-3}$	1.385	

momentum balance in the streamwise direction can then be evaluated thanks to the measurement of the pressure drop.

Radial velocity profiles and pressure drop are discussed in the third section. For each flow rate investigated, the velocity profiles are quite symmetric and suggest that the dense emulsion flow obeys a shear-thinning law with the same flow index $n = 1/2$ as that already observed in a wide-gap Couette cell.[15,17,22] This effective medium behavior is however not consistent with the evolution of the pressure drop with the mixture velocity, which is found to be linear instead of a square root law.

The origin of this apparent contradiction is analyzed in the fourth section through two mechanisms of different nature. The first is related to the evolution of consistency factor with drop size based on the experimental results of Pal[15] in a homogeneous Couette flow. In our case, drop size variation would be induced by the variation of pump rotation speed at different flow rates. The second originates from shear-induced diffusion and leads to the development of a weak gradient concentration profile in the flow section, independent of flow rate. Assuming a Newtonian behavior of the emulsion, the concentration profile deduced from the local momentum balance at steady state

(a)

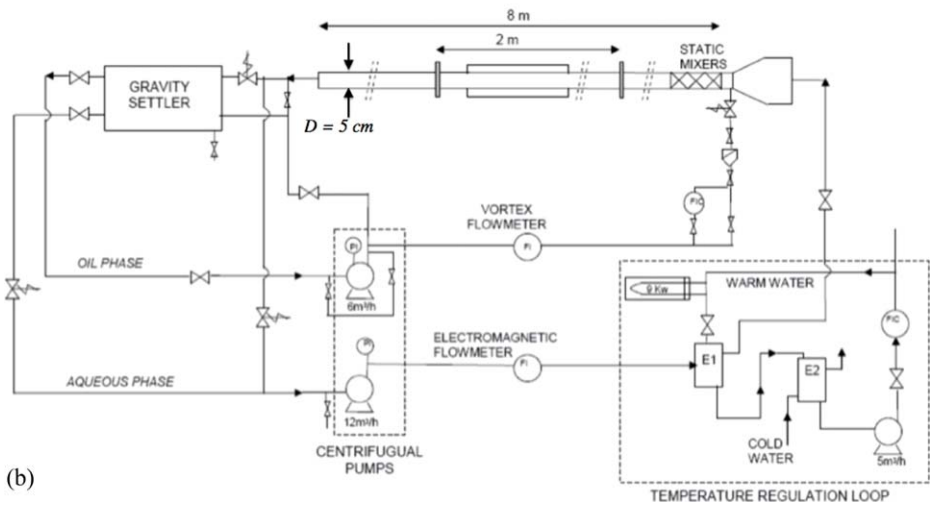

(b)

Figure 2. Overview (a) and schematic (b) of the experimental rig.

[Color figure can be viewed at wileyonlinelibrary.com]

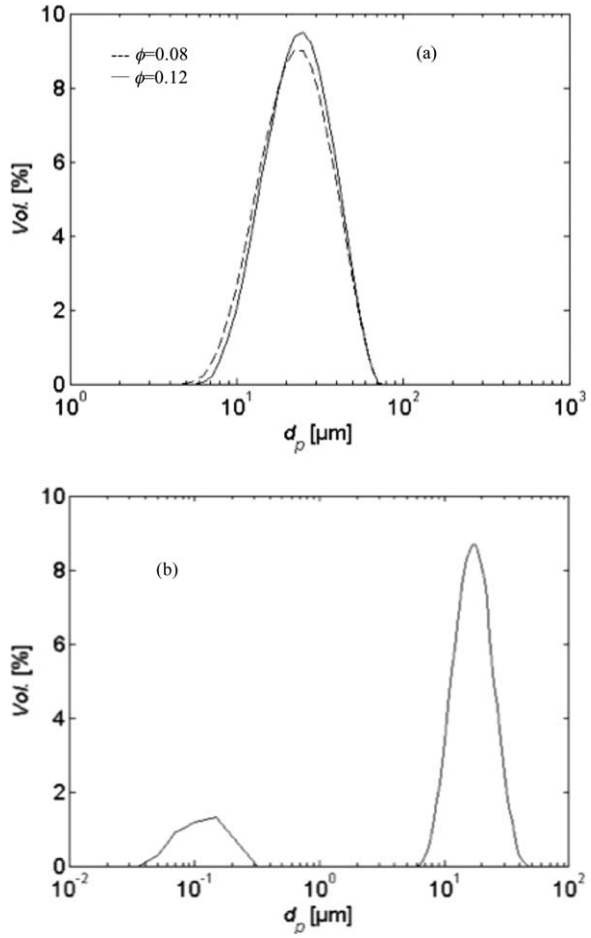

Figure 3. Drop size distribution at low concentration (a) $N = 1900$ rpm; (b) $N = 2400$ rpm.

Continuous line (oil volume fraction of 12%); dashed line (oil volume fraction of 8%).

is interpreted with the help of a simple Suspension Balance Model (SBM), as that proposed by Zarraga et al.[23] The applicability of this model to the present emulsion pipe flow is discussed in terms of drop deformability, length of establishment of the concentration profile, and sign of second normal stress difference. Last section regroups the main conclusions and perspectives of this work.

Experimental

Phase system

The o/w emulsion is composed of n-heptane as the dispersed phase and an aqueous solution of glycerin (43% v/v) as the continuous phase. At 29°C, refractive indices of both phases are matched ($n_D = 1.385$) allowing the implementation of PIV technique. Phase properties of the phases at 29°C are reported in Table 1.

Liquid-liquid rig and measuring techniques

The scheme of the experimental rig is reported in Figure 2. The device is composed of an 8-m long cylindrical pipe made of poly-methyl methacrylate (PMMA) of $D = 5$ cm internal diameter, a storage tank of 400 L from which the liquid phases are pumped toward the pipe, and a secondary loop that regulates the temperature in the pipe through a heat exchanger. The pipe is first filled with both phases at the desired volume concentration, and then the mixture is circulating in a closed loop in the water circuit, the emulsion being produced and transported by a centrifugal pump of variable rotation speed. For each test, the volume concentration ϕ_0 is *a posteriori* checked by settling an emulsion sample taken out from the pipe flow. The flow rate in the pipe is measured by an electromagnetic flowmeter (0.5% accuracy).

In the range of pump rotation speed used in this study, the mean drop diameter of the o/w emulsion is close to 20 μm (measured in rather dilute conditions).

The shape of the drop size distribution (measured by a laser granulometer) is found to be slightly sensitive to the pump rotation speed. As the latter increases between 2200 and 2800 rpm, the distribution (measured only for $\phi < 0.25$) shifts from a unimodal (Figure 3a) to a bimodal distribution (Figure 3b), resulting in a slight decrease of the mean drop diameter. Therefore, in the range of flow rates employed for this study, the emulsion is polydisperse.

The pressure drop is measured along the pipe with the help of a differential pressure gauge with a maximum uncertainty less than 10%. The velocity field in the emulsion is measured by PIV. A vertical laser sheet is generated in a median plane of the pipe at a distance $L = 3.3$ m (66 pipe diameter D) from the pipe inlet (Figure 4). The laser source is composed of a high-frequency double cavity of 10 mJ each at a wavelength of 527 nm. The flow is seeded with 20 μm PMMA particles with encapsulated Rhodamine B, a fluorescent dye that reemits light at a higher wavelength (584 nm). Volume fraction of

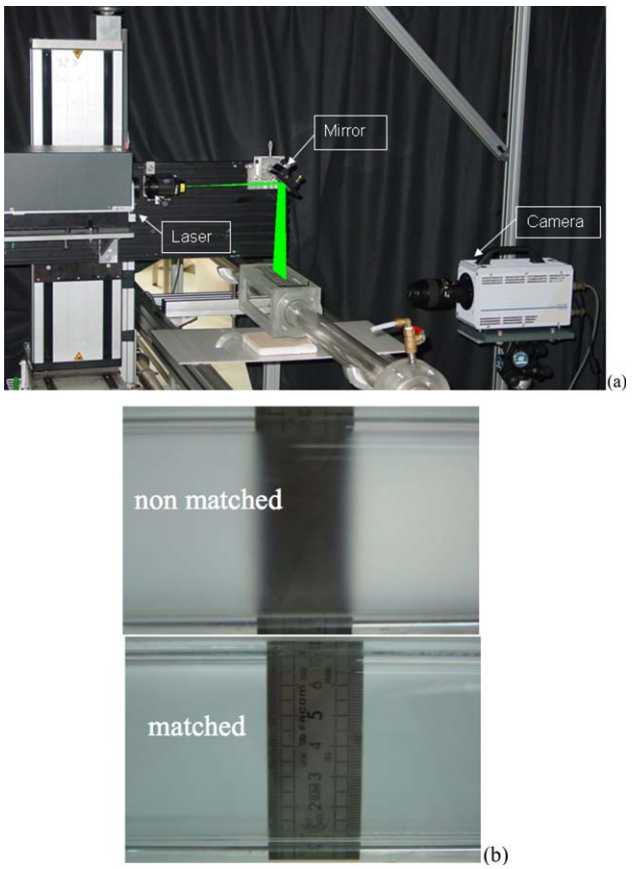

Figure 4. (a) PIV system implemented on the pipe; (b) illustration of phase index matching in the pipe flow.

[Color figure can be viewed at wileyonlinelibrary.com]

Table 2. Flow Parameters

U_m (m s^{-1})	0.56	0.7	0.85	1
N (rpm)	2200	2400	2400	2800
$\mathrm{Re}_m = \rho_m U_m D/\mu_m$	32	40	49	57
$\mathrm{Re}_p = \mathrm{Re}_m(\mu_m/\mu_c)(d_{32}/D)^2$ with $\mu_m = \mu_c(1-\phi/\phi_m)^{-2.5\phi_m}$	2.8×10^{-4}	3.5×10^{-4}	4.3×10^{-4}	5×10^{-4}

these particles is of the order of 10^{-5}, so there impact on emulsion flow is negligible. A high-speed video camera (RS3000 Photron®) with an image resolution of 1024 × 1024 pixels records the displacements of the seeding particles between two successive images at a spatial resolution of 0.9 mm (56 data points in a pipe diameter). The camera is equipped with a 100-mm lens and a high-pass filter (cut wavelength of 540 nm) to filter the incident wavelength. Statistical averages were performed over 2000 images corresponding to an integration time of about 4 s, which is quite enough in steady laminar regime (negligible velocity fluctuations).

Flow parameters

The volume concentration of the emulsion has been set to $\phi_0 = 0.70$ (± 0.02) in this study, beyond the range corresponding to a hard sphere behavior of the emulsion.[6] Four different mixture velocities U_m are investigated, involving different pump rotation speeds ($2200 < N < 2800$ rpm). Corresponding pipe Reynolds number based upon emulsion viscosity μ_m (using Newtonian law at $\phi = 0.7$) and particle Reynolds number based upon continuous phase viscosity μ_c, (for a Sauter diameter $d_{32} = 20$ μm) are reported in Table 2.

Although there is no surface-active species added to the system, the presence of contaminants is unavoidable (due to impurities in both phases and contamination due to flowing through the different elements of the rig) and interfaces are likely to behave as immobile interfaces (adhesion condition at the interface). As a result, inter-drop coalescence time is rather long, and even if the emulsion continuously separating with time, it takes more than one day for an emulsion sample to fully separate under gravity. Due to the small residence time (few tens of seconds) of the emulsion in the pipe between the pump outlet and the measuring section, the emulsion is unaffected by coalescence, even at high concentration.

Flow Velocity Profile and Pressure Gradient

As discussed in Pouplin et al.,[6] phase segregation can be visualized by the distribution of seeding particles in the pipe cross section. They are more concentrated in the zone where drops are more concentrated, leading to a grey level gradient in the pipe section. In the case of a 70% concentrated emulsion, no clear gradient of the seeding particle concentration could be detected, suggesting that, within a range of small concentration variation, the emulsion flow is *a priori* homogeneous at all flow rates studied. However, this assessment is only qualitative and must not be confused with an accurate measurement of the drop concentration profile in the cross section (see for instance, Refs. 16 and 21).

Axial velocity profiles

A typical instant velocity field is displayed in Figure 5a, for a mixture velocity of 0.85 m s^{-1}. The flow seems to be quite axisymmetric and parallel, corresponding to a fully laminar regime, which is confirmed in Figure 5b by the perfect coincidence of the axial velocity profiles taken at the two ends of this instant field (z denotes the vertical coordinate in a median plane along the pipe diameter). Note also that the velocity profile significantly deviates from a parabolic profile, with a quasi-flat shape near the centerline of the pipe section, characteristic of a shear-thinning behavior. This velocity profile is reproduced at all mixture velocities investigated as shown in Figure 6, where the axial velocity profiles $V_x(z/D)$ are reported (where x denotes the coordinate in the streamwise direction, radial coordinate r and vertical coordinate z are simply related through $r/R = z/R - 1$). In all cases, no significant velocity fluctuation has been measured, flows are fully laminar and established. Profiles are quite symmetric with a slight larger gradient close to the bottom wall than to the upper wall, which probably results from a slight drop concentration difference following the vertical direction. To illustrate the shear-thinning behavior, the parabolic profile has been plotted in the case $U_m = 1$ m s^{-1}.

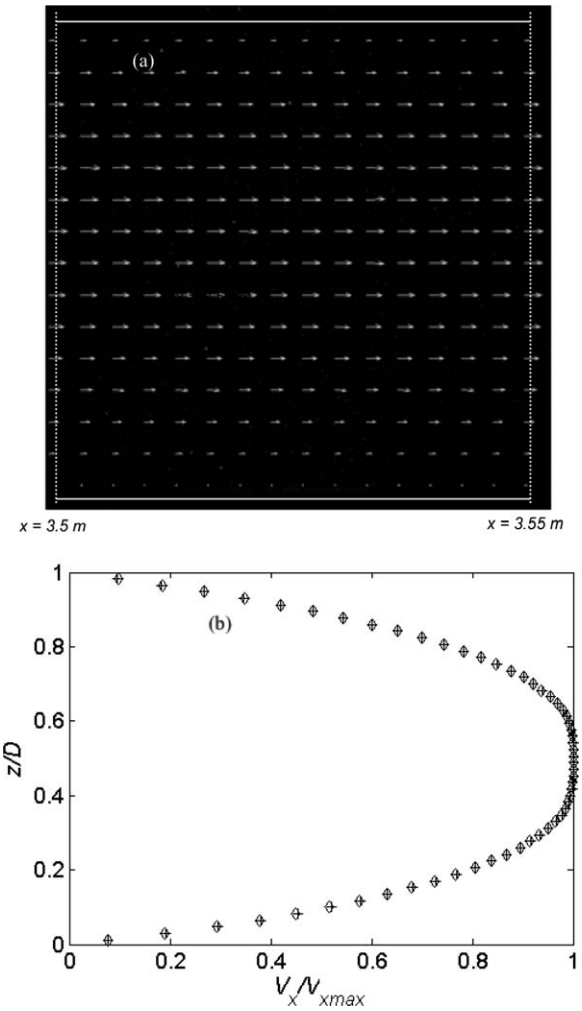

Figure 5. (a) Instant velocity field for $U_m = 0.85$ m s^{-1}; (b) axial velocity profiles at $x = 3.5$ m (¤) and $x = 3.55$m (+).

(z is the vertical coordinate along pipe diameter; $z/D = 0$: bottom wall; $z/D = 1$: upper wall; radial coordinate $2r/D = |2z/D\text{-}1|$ with $D = 2R$).

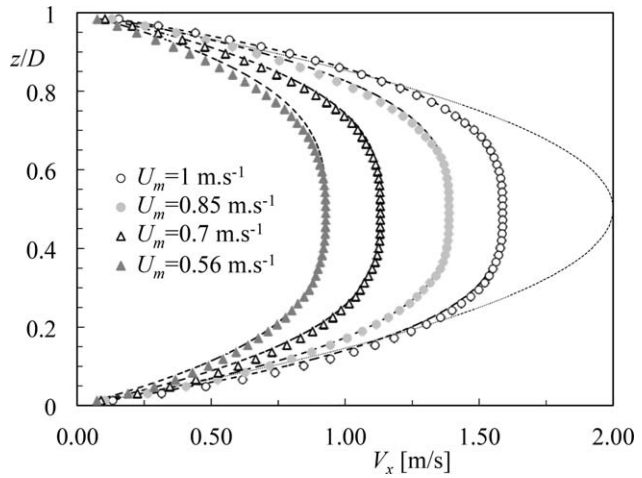

Figure 6. Axial velocity profiles in the cross section at different mixture velocities.

Dotted line is the parabolic profile at $U_m = 1$ m/s. Dashed lines correspond for each mixture velocity to the power law profile $V_x = V_{x\max}(1-|z/R-1|^{(n+1)/n})$ with $n = 0.5$. (z is the vertical coordinate along pipe diameter) V_{xmax} is the maximum velocity of V_x on the pipe centerline.

Assuming a quasi-homogeneous flow (i.e., no concentration gradient in the cross section) these velocity profiles can be used to derive the rheological law of the emulsion at this concentration.

The momentum balance in the streamwise direction x of a steady, laminar and established pipe flow, reduces to

$$\tau_{rx} = \frac{r}{2}\frac{dP}{dx} \tag{2}$$

where dP/dx is the established pressure gradient in the flow direction, which is constant for a given mixture velocity. Shear stress is hence proportional to the radial location in the pipe section, r. Plotting the radial position as a function of the radial derivative of the axial velocity therefore provides the emulsion stress–strain curve in real flow conditions. Normalized velocity gradient profiles $\left(\frac{dV_x}{dz}\frac{R}{U_m}\right)$ are reported in Figure 7a. They well collapse on a single curve, suggesting a single rheological behavior at all mixture velocities. It is clearly not a linear dependence but a power law (shear-thinning behavior) instead with an apparent yield stress, which can be deduced from the cancellation of the stress over a band of finite thickness near the centerline. When zooming in this region (Figure 7b), one observes that the width of this band is in reality smaller than the PIV resolution mesh size (0.0125D), which would correspond to a maximum yield stress τ_y of order of 1 Pa for the maximum pressure drop considered (1800 Pa m^{-1} at $U_m = 1$ m s^{-1}). Neglecting this quantity, stress–strain plots have been tested against Oswald's law

$$\tau_{rx} = \kappa|\dot{\gamma}|^{n-1}\dot{\gamma} \text{ with } \dot{\gamma} = dV_x/dr \tag{3}$$

where n is the flow index and κ the consistency factor. Substituting (3) in (2) and integrating along the radial direction provides the axial velocity profile

$$V_x(r) = V_{x\max}\left[1-(r/R)^{(n+1)/n}\right] \tag{4}$$

Equation 4 assumes a no-slip boundary condition at the wall. Note that the spatial resolution (0.6 mm) of the measured velocity profile does not allow determining precisely if there is a slip at the pipe wall, but in any case, its value would be smaller than a few percent at most of the mean velocity and can therefore be neglected. The profile of $1 - V_x/V_{x\max}$ in the cross section is reported in Figure 8a on a log–log scale for all mixture velocities. For each value of U_m, two curves corresponding to the upper and bottom section profiles have been plotted. Based upon Eq. 4, the slope of each curve is equal to $(n + 1)/n$ and therefore provides the flow index n. All profiles can be perfectly fitted by a power law with an exponent close to 0.5, which corresponds to the r^{*3} power law on this graph. The exponent corresponding to the upper section is always slightly larger than that of the bottom section, as a probable result of a slight difference in concentration. Another way to represent the data is to plot the apparent viscosity $\mu_a = \kappa|\dot{\gamma}|^{n-1}$ scaled by its wall value as a function of dimensionless shear rate $\dot{\gamma}^* = (dV_x/dr)(R/U_m)$

$$\begin{aligned}\mu^* &= \mu_a/\mu_{aw} = |\dot{\gamma}(r)/\dot{\gamma}(R)|^{n-1} \\ &= |[n/3n+1]\dot{\gamma}^*|^{n-1} = \sqrt{5/|\dot{\gamma}^*|} \text{ with } n=0.5\end{aligned} \tag{5}$$

Experimental data are reported in Figure 8b for both upper and bottom sections at each mixture velocity. Apparent viscosity has been normalized by the wall-averaged value between upper and bottom sections. It can be seen that all data well collapse on the same curve and well compare with Eq. 5 with a weak scattering. The point (5,1) on this graph represents the

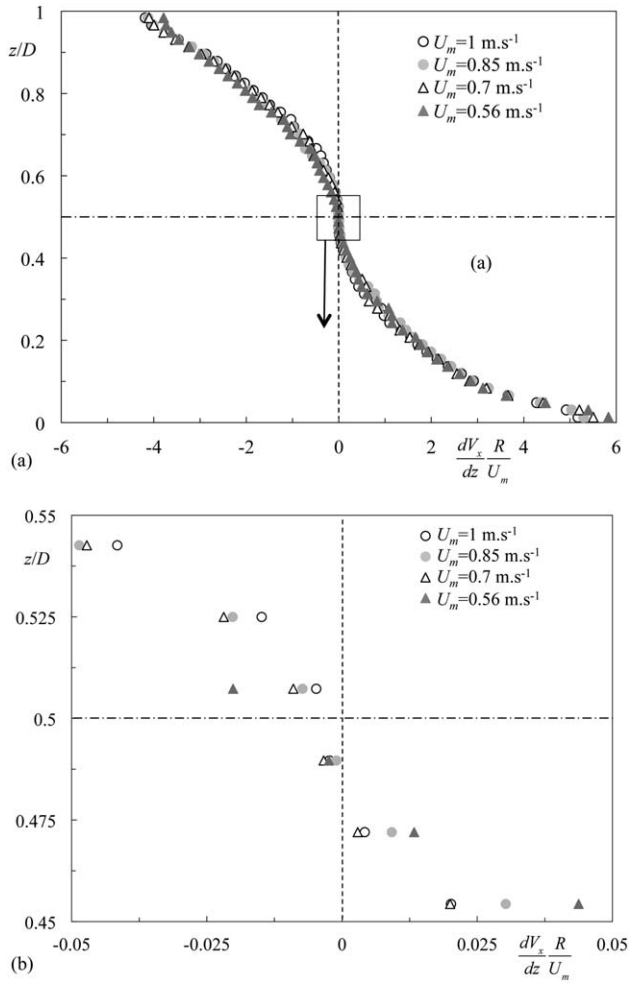

Figure 7. (a) Velocity gradient profiles in the cross-section at different mixture velocities (b) Zoom near the centerline. R is the pipe radius (=2.5cm).

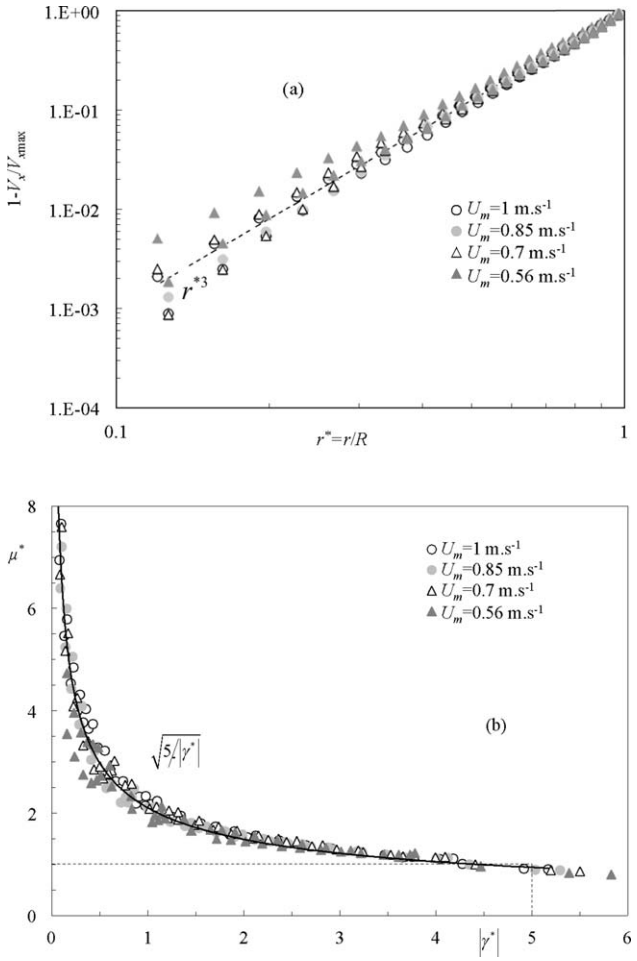

Figure 8. (a) Radial profile of 1 – V_x/V_{xmax}. For each U_m, the upper and bottom profiles have been reported.

Dashed line is $(r/R)^{(n+1)/n}$ $(=r^{*3}$ for $n=0.5$). (b) Apparent viscosity versus shear rate. Continuous line represents Ostwald's law with $n=0.5$ (the point (5,1) on this graph is the corresponding wall value).

wall value obtained with Eq. 5. A slight dispersion can be observed around this point due to the slight dissymmetry, but the agreement is overall quite good. This flow index value of 0.5 is consistent with literature data obtained in wide-gap Couette flow geometries for noncolloidal dense emulsions in the same range of drop size. Among those, Jager-Lézer et al.[22] have performed a detailed rheological analysis of concentrated o/w emulsions (of order few microns in size) with different techniques in a range of high concentrations (0.6–0.85). Their data show that the yield stress of the emulsion starts to develop rapidly in the range 0.65–0.7, increasing from 1 to several tens of Pa. In the range [0.6, 0.7], the shear stress of the emulsion is well described by a Herschel–Bulkley model with a flow index close to 0.5.

Salmon et al.[24] have identified a flow index of 0.4 ± 0.1 for a 75% concentrated nonadhesive o/w emulsion (2 μm drop diameter). In the same range of concentration (>0.7), Ovarlez et al.[16] confirmed the validity of the Herschel–Bulkley model with a constant flow index close to 0.5 for both adhesive and nonadhesive o/w emulsion of few microns in size.

Setting the flow index n to 0.5 in Eq. 3, consistency factor κ can be deduced combining Eqs. 2 and 3. Profiles of κ have

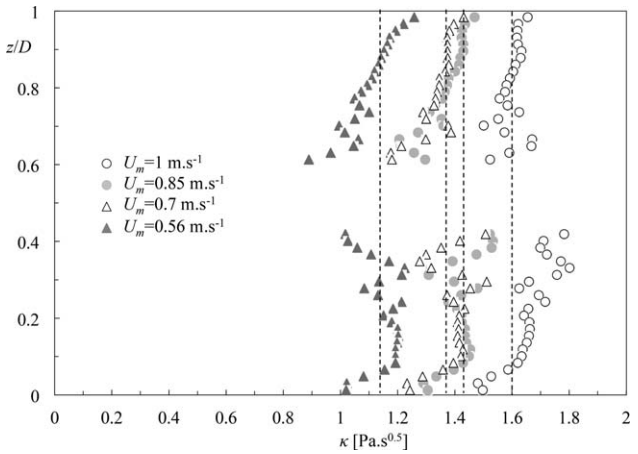

Figure 9. Profiles of consistency factor κ in the cross-section at different mixture velocities.

Vertical dashed lines represent the z-averaged value for each case (z is the vertical coordinate along pipe diameter).

been plotted in Figure 9 for all mixture velocities. As can be seen on this graph, a nearly constant value is obtained over the entire pipe section for each mixture velocity (except near the pipe center where consistency diverges because of the low values of the shear rate), confirming the good fit of emulsion rheology with Oswald's law. However, we note that the averaged values of κ over the pipe diameter increase from 1.1 to 1.6 Pa s$^{0.5}$ as the mixture velocity is increased from 0.56 to 1 m s^{-1}. As the consistency factor is not dependent of the local shear stress, its evolution can be ascribed to a modification of the emulsion microstructure when the flow parameters are changed. Numerical values of κ have been reported in Table 3 for the different flow parameters. We can see that the change of mixture velocity is accompanied with a variation of the pump rotation speed, which is increasing with the flow rate. As the emulsion is produced by the passage through the centrifugal pump, the slight modification of drop size distribution illustrated in Figure 3 can be responsible of an increase of interfacial area due to a diminution of Sauter diameter with the increase of the pump rotation speed, and consequently of an increase of the prefactor κ in Eq. 3. This point will be discussed later.

The values of the wall apparent viscosity have been also reported in Table 3. A slightly larger value is observed at the top wall compared to that of the bottom wall, possibly due to a slight sedimentation effect. The averaged value is close to 0.11 Pa s and surprisingly, it is found to be independent of mixture velocity, and therefore of the wall velocity gradient. Note that this value cannot be easily interpreted as the transition to a Newtonian regime at high shear rate that would lead, at a concentration of 70%, to a wall viscosity based upon Eq. 1, four to five times higher than that measured. Therefore, a

Table 3. Consistency Factor, Wall Apparent Viscosity, and Pump Rotation Speed for the Each Mixture Velocity Investigated

U_m (m s^{-1})	1	0.85	0.7	0.56
N (tr min^{-1})	2800	2400	2400	2200
κ (Pa s$^{0.5}$)	1.6	1.4	1.36	1.13
μ_{aw} (Pa s; top)	0.127	0.124	0.133	0.136
μ_{aw} (Pa s; bottom)	0.104	0.097	0.100	0.089
μ_{aw} (Pa s; average)	0.116	0.111	0.117	0.113

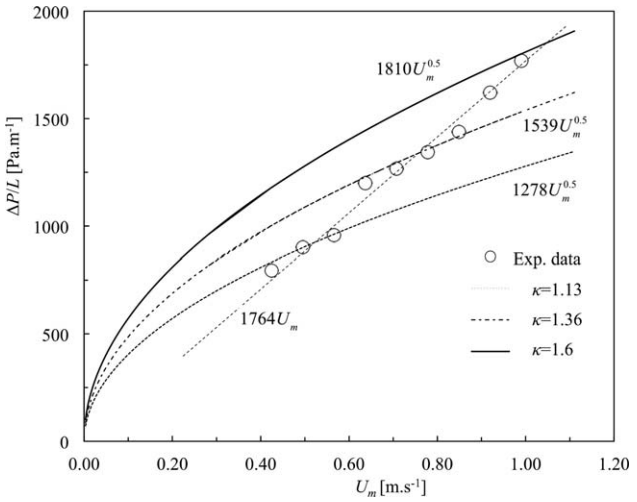

Figure 10. Pressure drop vs. mixture velocity.

Newtonian behavior of the emulsion involves the development of a concentration profile in the pipe section with a minimum at the wall and a maximum at the centerline.

Pressure drop

The pressure drop was measured at a distance equal to $66D$ ($= 122R$) from the pipe inlet and its evolution with mixture velocity is reported in Figure 10. For an Oswald's fluid, the pressure drop should vary like the mixture velocity to the power n (flow index), that is, as a square root law in the present case

$$\left|\frac{dP}{dx}\right| = 2\frac{\kappa}{R}\left(\frac{nV_{x\max}}{(n+1)^2R}\right)^n = 2\frac{\kappa}{R}\left(\frac{n(3n+1)U_m}{(n+1)^2R}\right)^n \qquad (6)$$

However, such a scaling assumes a constant value of the consistency factor at all flow rates, which is not the case here. Instead, Figure 10 exhibits a good linear fit of the pressure drop vs. the mixture velocity. To illustrate the effect of the variation of κ with U_m, the different pressure drop-mixture velocity curves have been reported in Figure 10 with the different values of κ identified.

The square root dependence clearly cannot properly represent the evolution of the pressure drop with the mixture velocity. The dependence of the pressure drop with U_m can be written using the apparent viscosity at the wall, μ_{aw}

$$\left|\frac{dP}{dx}\right| = \frac{2(3n+1)}{n}\frac{\mu_{aw}}{R^2}U_m \qquad (7)$$

The linear fit obtained from experimental data is therefore consistent with a constant value of the wall apparent viscosity and taking $n = 0.5$, the slope of the straight line gives $\mu_{aw} = 0.11$ Pa s.

Discussion

The linear evolution of the pressure drop is a typical macroscopic response of a Newtonian flow in a pipe, while the velocity field is a clear signature of local shear-thinning behavior. Both measurements could be mutually consistent by considering either a dependence of consistency factor on flow parameters for a fully homogeneous emulsion or a locally Newtonian behavior with the development of a concentration gradient in the flow section (i.e., a nonhomogeneous emulsion). These two modeling approaches are quite different in nature and their evaluation is an important issue regarding the scaling-up of transport processes. As the concentration profiles are not available in the present study as in Ovarlez et al.,[16] they cannot be discriminated and will be examined more thoroughly separately in this section. Aside from these two models, another possible mechanism would be to consider a homogeneous emulsion separated from the pipe wall by a lubrication film of continuous (aqueous) phase, as already evidenced by Briceño and Joseph[25] in pipe flows of concentrated foams. But it can be shown that the conservation of momentum would then require a velocity at the film-emulsion interface to be close to the mixture velocity (uniform plug flow), which is indeed verified in the case of dense foam flows but not in the present case, as demonstrated by the velocity profiles of Figure 6. This lubrication mechanism, even if present, has a negligible contribution to the momentum balance (which turns to be equivalent to neglect the slip velocity at the wall).

Homogeneous shear thinning

Assuming the flow to be fully homogeneous in the flow section leads to identify a variable consistency factor, which suggests a change in the emulsion microstructure when pump rotation speed is modified. It seems difficult to imagine a constitutive model able to identify the different contributions of the emulsion microstructure to the shear-thinning behavior on one hand and to the consistency factor (or apparent viscosity) on the other hand. What we have observed in our experiments is that the shear-thinning mechanism is approximately unchanged when the pump rotation speed is varied whereas the consistency factor is significantly affected. It is worth to mention here the study of Pal[15] on the effect of polydispersity on the rheology of concentrated emulsions in Couette devices. He showed that the relative viscosity data obtained with emulsions of different drop size distributions could be rescaled as a power law of a particle Reynolds number based on the velocity perturbation $\dot{\gamma}a_{32}$, where a_{32} is the drop Sauter radius and $\dot{\gamma}$ is the shear rate in the Couette cell

$$\mathrm{Re}'_p = \dot{\gamma}a_{32}^2/\nu_c \qquad (8)$$

Note that this Reynolds number should preferably be seen as the inverse of a Schmidt number that scales the drop shear-induced diffusion by the carrier fluid kinematic viscosity, ν_c. For a 70% concentrated o/w emulsion of micrometric nondeformable drops, the scaling of the relative viscosity (although not mentioned in the text of Pal's paper[15]) can be derived from a data set (Figure 7 in Pal's paper)

$$\mu_r = \mu_m/\mu_c \cong \mathrm{Re}_p'^{-0.5} \text{ for } 10^{-5} < \mathrm{Re}_p' < 10^{-2} \qquad (9)$$

From that relation, it can be deduced that the emulsion behaves as a shear-thinning fluid with a flow index of 0.5 and a consistency factor scaling as

$$\kappa \cong 3\mu_c\left(\frac{a_{32}^2}{\nu_c}\right)^{-0.5} = 3\left(\frac{\mu_c^3}{\rho_c}\right)^{0.5}\frac{1}{a_{32}} \qquad (10)$$

This relation indicates that for a flow index of 0.5, the consistency factor is inversely proportional to the Sauter radius of the drop, and most probably proportional to the interfacial area. Such a dependence has some physical grounds: for a given polydisperse concentrated system, if we admit that the flow index reflects an optimal rearrangement of the dispersion

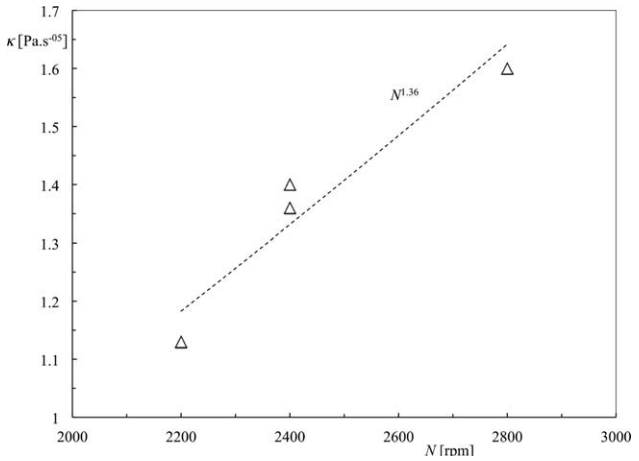

Figure 11. Consistency factor κ vs. pump rotation speed N.

to minimize the resistance to a shear stress, decreasing the average size of the emulsion while keeping the polydispersity index constant is not expected to modify the internal structure of this rearrangement under stress. In return, if we interpret κ as a scaling factor of a dissipation rate, increasing the interfacial area will increase the number of inter-drop lubrication films per unit volume, and hence increase the dissipation rate and the value of κ.

As the size and particle Reynolds number of the present emulsion lies in the same range as that of Pal's experiments, scaling relation 10 can be tested with our data. For an averaged drop radius of 10 μm, the expected value of κ in the 70% concentrated emulsion would be 1.63 Pa s, which has the same order of magnitude as the value identified from pressure drop measurements (see Table 3). It can be concluded that Eq. 10 extracted from Pal's data predicts the right order of κ in our experiments.

Next question is to know if the observed evolution of κ with pump rotation speed as the flow rate is increased is compatible with a reasonable estimate of rate of change of drop diameter. The emulsion being produced by the centrifugal pump, the main mechanism responsible of drop fragmentation is due to turbulence produced at the impeller tip. At high concentration, even if the radial flow between two consecutive blades is possibly laminar, the flow in the pump casing is probably turbulent, with a dissipation rate of turbulent kinetic energy ε scaling as N^3 (where N is the impeller rotation speed). Following Kolmogorov's theory, in the inertial range, drops maximum stable diameter will be scaled by $\varepsilon^{-0.4}$, whereas in the sub-Kolmogorov range it will be scaled by $\varepsilon^{-0.5}$. By extension, the evolution of averaged drop radius a_{32} with N is expected to scale as $N^{-1.2}$ or $N^{-1.5}$, and hence κ will scale like $N^{1.2}$ or $N^{1.5}$ from Eq. 10. As illustrated in Figure 11, fitting the values of κ by a power law of N leads to

$$\kappa \propto N^{1.36} \tag{11}$$

Even if not accurate, the exponent is comprised between 1.2 and 1.5, suggesting that this evolution is consistent with a dependence of κ with drop diameter in our experiments. Note that according to this trend, between 2200 and 2800 rpm the mean drop diameter would only vary between 20 and 15 μm.

As a conclusion, a homogeneous shear-thinning fluid of flow index 0.5 is a correct representation of the 70% o/w emulsion if the dependence of the consistency factor with the interfacial area can be established. A scaling law derived from an experimental data set of Pal[15] and the estimation of drop size evolution with pump rotation speed both provide a good level of prediction of κ, and thus a possible explanation of the observed linear evolution of pressure drop with the flow rate. However, at concentrations above the glassy transition (i.e., with significant nonzero value of the yield stress), Ovarlez et al.[16] have identified a Herschel–Bulkley's model with a flow index of 0.5 and a consistency factor that is not related to the mean size of the drops. Therefore, if this dependence of κ with the drop size exists, it seems to be only valid in a limited range of concentration below the glassy transition.

Shear-induced migration

The second emulsion model assumes that the shear viscosity of the 70% concentrated emulsion is Newtonian and that its dependence with local concentration is given by Eq. 1. This assumption is supported by the fact that the micron sized droplets have a small Capillary number ($Ca_{\max} = \mu_c \dot{\gamma}(R) a_{\max}/\sigma \cong O(10^{-4})$) based on the maximum shear rate ($\dot{\gamma}(R) \cong 200\ \mathrm{s}^{-1}$) and the maximum drop size ($a_{\max} \cong 30$ μm), so deformation-related effects are *a priori* negligible. Hence, it is likely that the emulsion behaves as a suspension of polydisperse smooth spherical particles. As aforementioned, the value of the apparent viscosity identified at the wall suggests that the concentration is smaller than 70%. Mass conservation therefore involves the development of a negative gradient of concentration in the radial direction. This concentration profile $\phi(r)$ can be deduced from the experiments and the momentum balance at any radial position r

$$\tau_{rx} = \frac{r}{2}\frac{dP}{dx} = \underbrace{\mu_c \mu_r(\phi(r))\dot{\gamma}(r)}_{\text{Newtonian model}} = \underbrace{-\tau_y + \kappa|\dot{\gamma}(r)|^{n-1}\dot{\gamma}(r)}_{\text{Experimental fit}}$$
$$\text{with } \dot{\gamma}(r) = 0 \text{ if } 0 \le r \le r_0, \tag{12}$$
$$\tau_y = -\frac{r_0}{2}\frac{dP}{dx} \text{ and } \mu_r(\phi(r)) = (1-\phi(r)/\phi_M)^{-2.5\phi_M}$$

In Eq. 12, although written in same form, the right-hand side term here no longer represents a Herschel–Bulkley model of the emulsion rheology but must be seen as an experimental fit of the shear stress in the radial direction. The concentration profile in the pipe section can then be deduced at each radial location from that equation. In the experimental fit of the shear stress profile, a possible nonzero value of the shear stress near the centerline is introduced to study the sensitivity of the concentration profile to this quantity (that would correspond to a yield stress in the Herschel–Bulkley model), threshold parameterized by a radial distance r_0 below which the shear rate cancels. Due to mass conservation requirements, this threshold value of the shear stress cannot exceed the order of 1 Pa, corresponding to a maximum value of r_0/R of the order of 5×10^{-2} (at $U_m = 1$ m s^{-1}). Concentration profile can then be deduced according to

$$\phi(r) = \phi_M \left(1 - \left[\frac{-\tau_y + \kappa|\dot{\gamma}(r)|^{n-1}\dot{\gamma}(r)}{\mu_c \dot{\gamma}(r)}\right]^{\frac{-1}{2.5\phi_M}}\right) \text{ and} \tag{13a}$$
$$\phi(r) = \phi_M \text{ for } 0 \le r \le r_0$$

which can be also expressed as a function of $r_0^* = r_0/R$

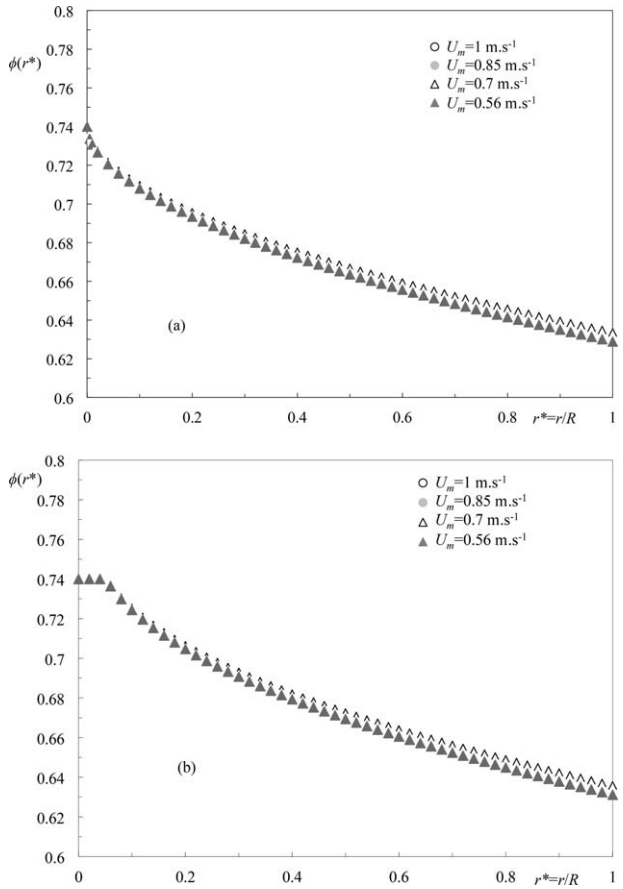

Figure 12. Dispersed phase concentration radial profiles from Eq. 13.

(a) $r_0^*=0$; (b) $r_0^* = 5 \times 10^{-2}$.

$$\phi(r^*)=\phi_M\left\{1-\left[\frac{\kappa}{\mu_c}\left(\frac{n+1}{n}\frac{V_{x\max}}{R}\right)^{n-1}\left(\frac{r^*-r_0^*}{1-r_0^*}\right)^{\frac{1}{n}}\frac{r^*}{\left(1-r_0^*\right)^n}\right]^{\frac{-1}{2.5\phi_M}}\right\}$$

$$\text{and } \phi(r^*)=\phi_M \text{ for } 0 \le r^* \le r_0{}^* \tag{13b}$$

This profile is plotted in Figure 12 for all mixture velocities with $n = 0.5$ and $\phi_M = 0.74$ and for $r_0^* = 0$ (Figure 12a) and $r_0^* = 5 \times 10^{-2}$ (Figure 12b). As a first observation, all profiles are independent of the mixture velocity and a unique function of r^* is obtained, resulting from the fact that in Eq. 13b, the product $\kappa V_{x\max}^{n-1}$ is nearly independent of the mean flow mixture velocity. Concentration is decreasing from ϕ_M at the centerline or below r_0^* to a constant value at the wall ϕ_R close to 0.63. It can be verified that at this concentration, the emulsion viscosity given by Eq. 1 is equal to 0.11 Pa s, which is the same value as that deduced from the slope of the Pressure drop-mixture velocity straight line, (cf. Figure 10). In the limit of acceptable range, the effect of the threshold value is limited to the near-axis region and its effect on the wall value is negligible. The integration of the local mass flux in the section (local concentration x local velocity) leads to an average concentration of 0.67, which is very close to the concentration of the emulsion (0.7 ± 0.2), a result that is obtained independently from any mass balance constraint and which brings some support to the shear viscosity model. Also, it is interesting to note that the gradient along this profile is smooth and that the concentration difference between the wall and the centerline is only 0.1. In this range of concentration, the emulsion viscosity as modeled by Eq. 1 is highly sensitive to the concentration and a relatively small variation of concentration is enough to shift a parabolic velocity profile (that would be obtained with a Newtonian emulsion without any concentration gradient) toward a cubic power law profile (cf. Figure 8a). This small concentration gradient also explains why it is not detectable by the grey level based on discrimination technique developed in Pouplin et al.[6] Similar observations were reported for dense suspensions with rigid particles in Couette[21] and pipe flows.[26] For example, in Couette flow, particles migrate toward the outer cylinder (where the shear rate is the lowest), and the concentration profile is dependent on the average concentration value but independent of the rotation velocity at a given average concentration of particles.

In the absence of inertia, the only mechanism from which this concentration gradient may result is shear-induced migration, which drives the dispersed matter from the high to the low shear zones, from the pipe wall toward the centerline in the present case. Since the early work of Leighton and Acrivos,[27] shear-induced diffusion has been extensively studied and evidenced in suspension flows of different geometries and can be modeled using diffusing flux formulation or

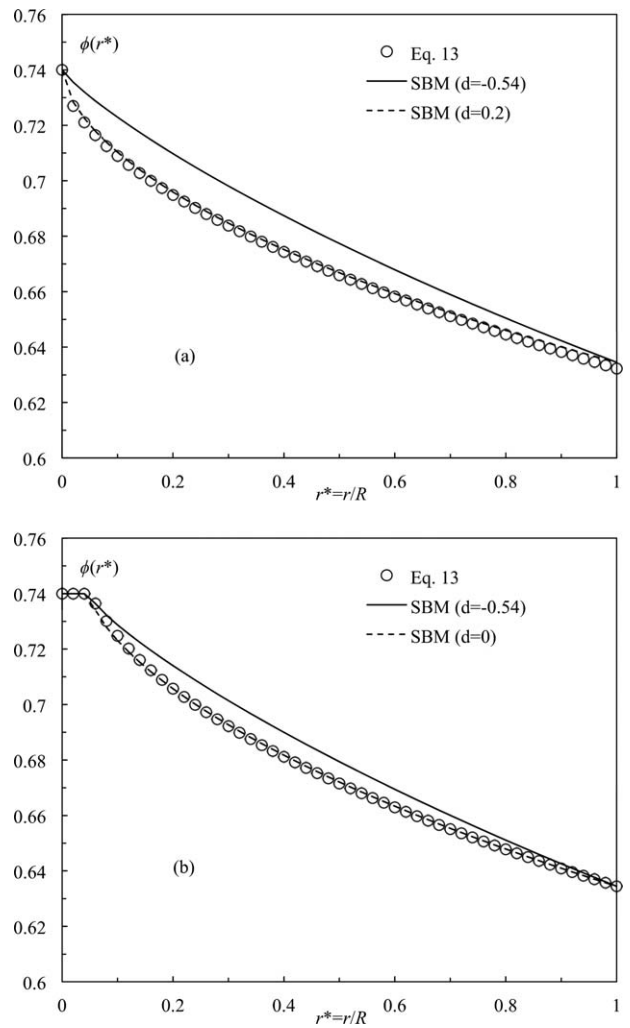

Figure 13. Comparison of SBM predictions (Eq. 14) with theoretical profile of ϕ as derived from Eq. 13.

(a) $r_0^* = 0$; (b) $r_0^* = 5 \times 10^{-2}$.

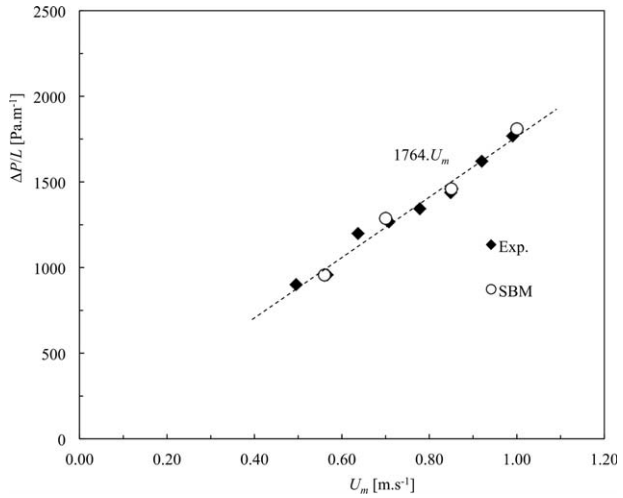

Figure 14. Evolution of pressure drop with mixture velocity.

Comparison between experiments and SBM prediction.

SBMs.[23,27–30] The derivation of the concentration profile in the flow section is detailed in the Supporting Information Appendix, using the SBM approach and constitutive laws of Zarraga et al.[23] for the emulsion rheology. The concentration profile then reads

$$\phi(r^*)=\frac{\phi_M h(r^*)}{\phi_M/\phi_R-1+h(r^*)} \text{ with } h(r^*)=r^{*d/3}\left[\frac{1-r_0^*}{r^*-r_0^*}\right]^{1/3n} \text{ for } r^* > r_0^* \text{ and } \lim_{r^*\to r_0^*}\phi(r^*)=\phi_M \tag{14}$$

This profile, which is not dependent upon flow velocity, is reported in Figure 13. It is compared, for different values of d, to the theoretical profiles of Figure 12, derived from the experimental velocity field data and assuming a Newtonian shear viscosity in the momentum balance (Eq. 12). The SBM profile remarkably fits these profiles for a value of d close to zero or even slightly positive. The profile corresponding with $d = -0.54$ has a close trend but slightly overestimates the theoretical profile. There is little effect of a stress threshold value which seems to shift the best fitting value of d from 0.2 to 0 when r_0^* is increased from 0 to 5×10^{-2}. This result means that the shear-induced migration mechanism as described by the SBM is consistent with a nearly fully Newtonian suspension, that is, with a Newtonian (concentration dependent) shear viscosity and a quasi-null second normal stress difference.

Evolution of pressure drop with mixture velocity as predicted by the SBM is identical as that given by Eq. 12 in $r = R$. In this case, pressure drop is obtained from Eq. 7 by substituting the apparent wall viscosity by the emulsion shear viscosity at $\phi = \phi_R \cong 0.63$, which is found to be independent of mixture velocity

$$\left|\frac{dP}{dx}\right|=\frac{2(3n+1)}{n}\frac{\mu_c}{R^2}(1-\phi_R/\phi_M)^{-2.5\phi_M}U_m \tag{15}$$

This relation is plotted in Figure 14 and confirms the consistency between shear-induced migration mechanism with the local velocity field and pressure drop experimental data. However, the relevance of such mechanism in the present study needs to be addressed, which comprises different questions.

First of these is the correspondence between emulsion drops and solid particles in the present case, which involves drop deformation and boundary condition for shear stress at the drop interfaces. Deformation of drops can be evaluated based upon an estimation of particle phase pressure Π, assuming an isotropic structure (normal stress components identical). According to Zarraga et al.'s models, particle phase pressure will be given by

$$\Pi(r)=\frac{1}{3}\sum_{ii}^{p}(r) \cong -\alpha(r)\tau(r)=-\mu_c\left[\frac{\phi(r)}{1-\phi_r/\phi_M}\right]^3\dot{\gamma}(r) \tag{16}$$

A local capillary number Ca® can be defined according to

$$Ca(r)=\frac{|\Pi(r)a_{32}|}{2\sigma}\cong\frac{1}{2}\left[\frac{\phi(r)}{1-\phi_r/\phi_M}\right]^3\frac{\mu_r\dot{\gamma}(r)a_{32}}{\sigma} \tag{17}$$

This Capillary number is reported in Figure 15 for a 10 μm Sauter radius. It grows from zero at the centerline to a maximum value at the wall, which is below 10^{-2} at the maximum mixture velocity investigated.

Even if the drops deformation is expected to be small in that regime, it is difficult to estimate the effect of this small but finite Capillary number on the emulsion rheology and radial migration, especially in that range of concentration. Lowenberg and Hinch[31] first achieved a numerical study on shear flow of deformable and concentrated drops (up to 30% in volume) and Zinchenko and Davis[32] did a similar work (but with a different method) up to 55% in volume. They have shown that emulsion shear viscosity is a decreasing function of Ca, and that shear-thinning is sensitive at small values of Ca ($0.025 < Ca < 0.3$). Also, they find that the first normal stress difference is positive and is a growing function of Ca, whereas N_2 is found to be negative at very small values of Ca (0.025) but its absolute value is a weak increasing function of Ca. As a consequence, at high concentration, there is a strong increase of normal stress differences intensity between $Ca = 0$ and a small value of $O(10^{-2})$. However, it is difficult to extrapolate their results to the present case, since these simulations are performed with clean interfaces (continuity of tangential stress is assumed at the interfaces) and are sensitive to the viscosity ratio.

Then deformability of drops generates an additional convective contribution to the radial flux as first studied by Chan and

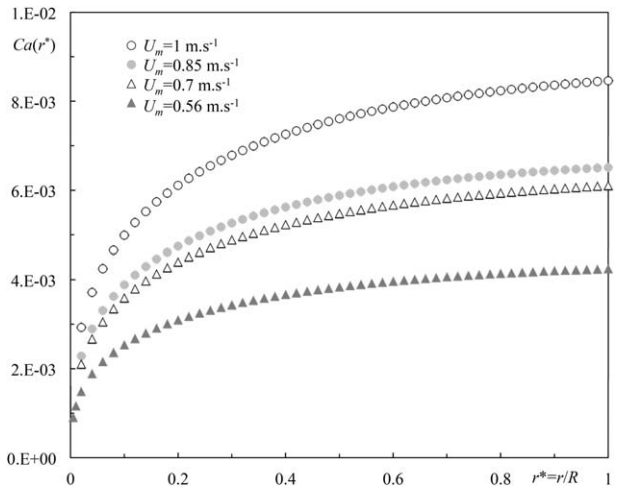

Figure 15. Capillary number as function of radial position in the pipe cross section.

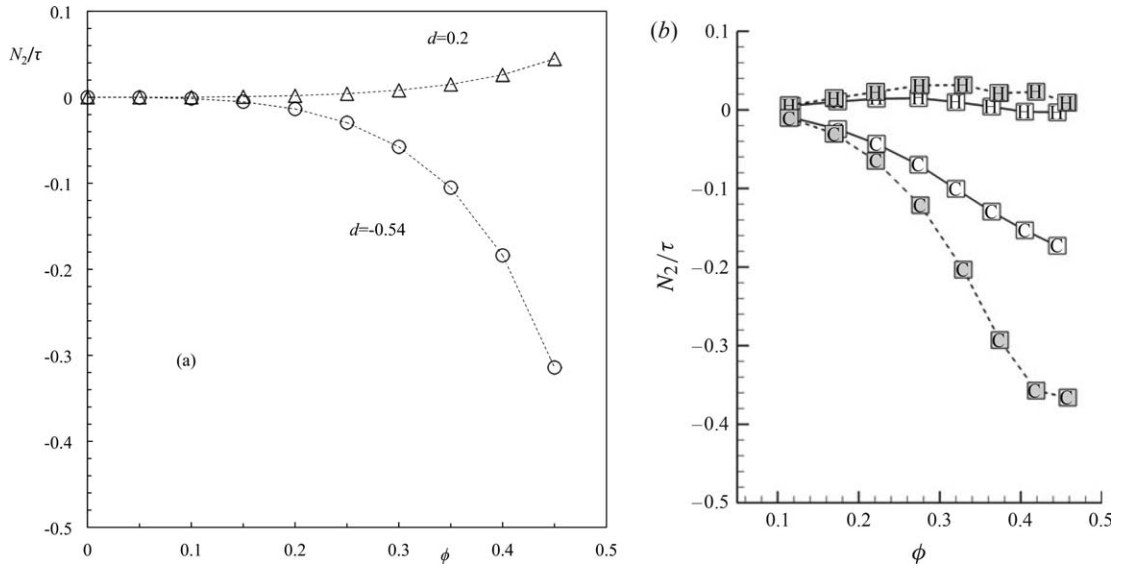

Figure 16. Evolution of N_2 with concentration.

(a) Present model derived from Zarraga et al.'s closure law (Eq. 21) with $d = -0.54$ and $d = 0.2$ ($d = 0$ corresponds to $N_2 = 0$). (b) Gallier et al.'s simulations in monodispersed sheared suspensions (Figure 13b from Gallier et al. JFM 757 (2014), doi:10.1017/jfm.2014.507). Letter C stands for contact forces contributions and H for hydrodynamic forces contribution. White symbols correspond to zero friction force and dark symbols to a friction coefficient of 0.5 (tangential to normal contact force ratio).

Leal[33] for an isolated drop. In the limit of dilute emulsions, Ramachandran et al.[34] have included this contribution in a SBM model where they have identified the particle stress components based on Lowenberg and Hinch[31] and Zinchenko's[35] works. The solution in a Poiseuille flow leads to the establishment of a concentration profile with a near-wall region free of droplets when the deformation-induced radial convection exceeds a critical value. Again, this term is highly sensitive to the viscosity ratio and is therefore limited to the case of clean interfaces. With contaminated interfaces, as it is the case in the present study, or with surfactants that are generally present in emulsions, the viscosity ratio could be no longer relevant or taking an infinite value of this ratio would be more appropriate. Doing so, in the estimated range of Capillary number of the present study ($10^{-3} < Ca < 10^{-2}$), it is expected that the contribution of deformation to the emulsion rheology is not significant, but this point requests a dedicated study with adequate rheological measurements. Another argument is that in Pouplin et al.,[6] the shear viscosity of the same emulsion was verified to be Newtonian and well compares with a suspension behavior up to a concentration of 56% (Figure 1b). Maximum Capillary number as estimated by Eq. 17 was of order $O(10^{-3})$ for that case, lying in the (lower range) of present experiments.

Assuming deformation to have a negligible effect, the second question to be addressed is the meaning of a zero or slightly positive second normal stress difference N_2, which is not expected for suspensions of rigid particles, where both N_1 and N_2 are negative and their absolute value is an increasing function of concentration. In a detailed numerical study of concentrated sheared suspensions, Gallier et al.[36] have decomposed the total stress components into hydrodynamic and nonhydrodynamic contributions as a function of concentration for different values of friction coefficient and surface roughness. In particular, their results show that the main contribution to N_2 is due to contact forces, while hydrodynamic part is negligible. It is worth noting that this hydrodynamic contribution to N_2 is slightly positive and nearly independent of concentration and friction parameter. The relative weight of these contributions is reversed for N_1, with $|N_1| < |N_2|$. In Figure 16, we have compared the evolution of the normalized value of N_2 with the concentration as predicted by Zarraga et al.'s model with the numerical predictions of Gallier et al.[36] of hydrodynamic and contact forces contributions.

It can be observed that the negative value of d in Figure 16a corresponds to the contribution of contact forces in Figure 16b, which intensity depends on friction coefficient, whereas a slightly positive value of d in Figure 16a would correspond to the hydrodynamic contributions in Figure 16b. Therefore, the range of values of d identified with the present system ($0 < d < 0.2$) could be interpreted as the signature of a suspension of smooth spherical drops separated by a lubrication film and with negligible contact forces. It can be also considered that polydispersity is likely to change drastically the rheological behavior of the suspension compared to the monodisperse case, in particular the radial pair distribution function that would have an impact on the normal stress differences.

The last question to be addressed is the length of establishment L_e of the concentration profile in the pipe resulting from shear-induced migration. To estimate this quantity, we simply write the equality between the residence time in the pipe L_e/U_m and the time of diffusion-induced migration over the pipe radius R, which scales as R^2/D_s, where D_s is the shear-induced diffusion coefficient

$$D_s = a^2 \frac{U_M}{R} D_s^*(\phi) \tag{18}$$

For a given geometry and particle (or drop) size, the length of establishment is then a function of ϕ, which can be written in dimensionless form as

$$L_e^* = \frac{L_e}{R}\left(\frac{a}{R}\right)^2 \propto \frac{1}{D_s^*(\phi)} \tag{19}$$

Experimental data have been collected at few meters from the pump outlet O(10m). As $(a/R)^2$ is $O(10^{-7})$, then Eq. 19 leads to

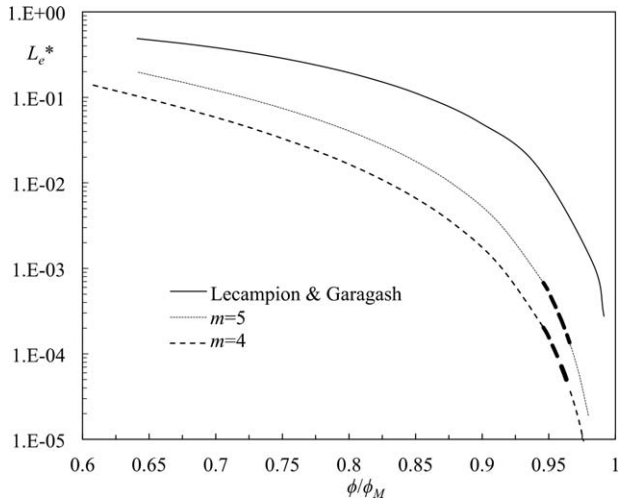

Figure 17. Evolution of length of establishment as a function of concentration derived from model of Lecampion and Garagash.[24]

Continuous line represents the calculation for monodisperse suspension. Dashed lines represent the estimation with present system for two different values of the exponent of the hindering function $f(\phi)=(1-\phi)^m$. Thick dashed lines correspond to the range of uncertainty of L_e^* with the present experiments.

$$10^{-4} < O\left(L_e^*\right) < 10^{-5} \tag{20}$$

which requests that the dimensionless shear-induced diffusivity is a strong increasing function of ϕ. Following Lecampion and Garagash,[26] it's possible to estimate the length of establishment of the concentration profile in the pipe

$$L_e^* = \frac{3}{8}\frac{(1+d)}{\phi^2}\frac{(1-\phi_r/\phi_M)^4}{3+2.5\phi}(1-\phi)^{-m} \tag{21}$$

in which m is the exponent of the hindering function (Eq. A2 in Supporting Information Appendix). Evolution of L_e^* as a function of ϕ/ϕ_M is reported in Figure 17. It can be observed that it is a strongly decreasing function of ϕ/ϕ_M, and the rate of decay is also a growing function of ϕ/ϕ_M, dropping over two orders of magnitude when ϕ/ϕ_M varies between 0.92 and 0.97. We also observe that these curves are sensitive to the hindering function exponent m. Thick dashed lines represents the range of values for the present experiments, accounting for measurement uncertainty of ϕ ($\phi/\phi_M \cong 0.95 \pm 0.025$). It can be seen that the range of values given by Eq. 21 fits with the condition expressed in Eq. 20.

From these trends, it can be concluded that the establishment of the radial profile of volume fraction over a few meters length is possible. It also explains why it was not observed at lower concentration in laminar regime[6] at the same measuring section in the pipe (few meters). Note that polydispersity also probably influences this length of establishment, because of aforementioned effect on emulsion rheology and also due to its probable effect on the hindering function.

It can be concluded that shear-induced migration is a possible effective mechanism in the present study and in the absence of accurate measurements of concentration profile, there is no way to discriminate it from the homogeneous shear-thinning scenario with an interfacial area dependent consistency factor. However, Ovarlez et al.[16] have measured the concentration profile of highly concentrated emulsions (volume fraction of 0.73, 0.75, and 0.88) in a wide gap flow cell and they did not observe any gradient resulting from a migration effect but a quite uniform distribution of drops in the gap. And this result was obtained with a well-marked velocity gradient profile in the gap. With concentrated suspensions, they had observed a concentration profile in the same Couette apparatus.[21] One possible explanation proposed by the authors is that deformation is no longer negligible in their systems and even small, it is responsible for inhibiting the development of normal stresses. Close to jamming, migration process would then be stopped or slowed down. Therefore, if shear-induced migration is involved in concentrated emulsions, its range of existence seems to be limited at high concentration due to drop deformation.

Concluding Remarks

The flow of a 70% concentrated o/w emulsion in a pipe has been investigated by means of Particle Image Velocimetry in a matched refractive index medium. The emulsion is polydisperse and mean drop diameter measured in more dilute conditions is about 20 μm. Velocity profiles are symmetric but not parabolic, suggesting a non-Newtonian behavior of the emulsion. For a steady established flow, the derivation of the shear rate profile in the section provides a stress–strain relation from which the rheological behavior can be identified. At all velocities investigated, it is well described by a Herschel–Bulkley model with a flow index of 0.5 and a nearly null yield stress, which is consistent with the literature data obtained in Couette flow devices in the same range of concentration. The consistency factor is a growing function of the mixture velocity, suggesting a possible variation of emulsion microstructure with flow parameters, and more specifically of the drops interfacial area with the pump rotation speed. Moreover, the linear dependence of pressure drop with mean velocity contradicts the expected behavior of a homogeneous fluid possessing these rheological properties that should exhibit a square root dependence instead. Two scenarios of different nature have been investigated and both seem to be consistent with the experimental observations.

First assumes that the fluid is indeed a homogeneous shear-thinning fluid and that relative viscosity can be scaled as the particle Reynolds number to the power -0.5 as experimentally observed by Pal.[15] This scaling implies a dependence of consistency factor with the inverse of the drop diameter. Estimation of κ with this scaling law gives the same order of magnitude as that measured in the present study. The possible evolution of drop diameter with pump rotation speed, based on a classical modeling of drop break-up in turbulent flow, is consistent with the observed evolution of κ. According to this modeling of κ, the linear evolution of pressure drop with mixture velocity would therefore result from the increase of κ with the pump rotation speed.

The second involves shear-induced migration, which satisfies both mass and momentum balance, considering a Newtonian behavior of the shear viscosity of this emulsion (using a Krieger–Dougherty's type law). In the considered range of Capillary number, drops are nearly spherical particles and deformation can be safely neglected. The concentration profile, resulting from the local experimental momentum balance, is well described by a SBM as proposed by Zarraga et al.[23] Concentration decreases from the maximum packing fraction at the centerline (0.74) to 0.63 at the wall, independently from the mixture velocity. This model is consistent with the

experimental velocity profile and the linear pressure drop evolution with mixture velocity. The best fitting between the SBM and theoretical profile issued from the experimental data corresponds to a zero or slightly positive value of second normal stress difference. Comparison with rheology of suspension of solid rough particles[36] suggests that the main contribution to the normal stress in the present emulsion is due to hydrodynamic interactions. The emulsion could be seen as a suspension of smooth particles separated by a lubrication film with no contact forces. An estimation of the length of establishment of the profile derived from Lecampion and Garagash's model[26] makes possible the development of this concentration profile in the present experiments. If both mechanisms considered here can explain quantitatively the experimental data they don't lead to the same results in terms of scaling up or down of such emulsion flows. Due to shear-induced migration, a given phase system could exhibit a Newtonian behavior in short pipe of large radius and a non-Newtonian behavior (shear thinning) in a long pipe of small radius. Interestingly, data of Ovarlez et al.[16] collected in concentrated emulsions above the glassy transition, do not confirm any mechanisms considered in this study, the dependence of the consistency factor with mean drop size and the shear-induced migration as well. It is therefore probable that the observed and sometimes contradictory behaviors of emulsions near the glassy transition are highly sensitive to the Capillary number based on the local granular pressure.

Literature Cited

1. Derkach SR. Rheology of emulsions. *Adv. Colloid Interface Sci.* 2009;151:1–23.
2. Datta SS, Gerrard DD, Rhodes TS, Mason TG, Weitz DA. Rheology of attractive emulsions. *Phys. Rev. E.* 2011;84:041404
3. Cohen-Addad S, Höhler R. Rheology of foams and highly concentrated emulsions. *Curr. Opinion Colloid Interface Sci.* 2014;19:536–548.
4. Blondin L, Doubliez E. Particle imaging velocimetry of a wet aqueous foam with an underlying liquid film. *Exp. Fluids.* 2002;32:294–301.
5. Meeker S, Bonnecaze R, Cloitre M. Slip and flow in pastes of soft particles: direct observation and rheology. *J. Rheol.* 2004;48(6):1295–1320.
6. Pouplin A, Masbernat O, Décarre S, Liné A. Wall friction and effective viscosity of a homogeneous dispersed liquid–liquid flow in a horizontal pipe. *AIChE J.* 2011;57(5):1119–1131.
7. Bécu L, Grondin P, Colin A, Manneville S. How does a concentrated emulsion flow? Yielding, local rheology, and wall slip. *Colloids Surf. A: Physicochem. Eng. Aspects.* 2004;263:146–152.
8. Pal R. On the flow characteristics of highly concentrated oil-in-water emulsions. *Chem. Eng. J.* 1990; 43:53–57.
9. Masalova I, Malkin AY, Slatter P, Wilson K. The rheological characterization and pipeline flow of high concentration water-in-oil emulsions. *J. Non-Newtonian Fluid Mech.* 2003;112:101–114.
10. Choi SJ, Showalter WR. Rheological properties of nondilute suspensions of deformable particles. *Phys. Fluids.* 1975;18(4):420–427.
11. Pal R. Viscous behavior of concentrated emulsions of two immiscible Newtonian fluids with interfacial tension. *J. Colloid Interface Sci.* 2003;263:296–305.
12. Yaron I, Gal-Or B. On viscous flow and effective viscosity of concentrated suspensions and emulsions. Effect of particle concentration and surfactant impurities. *Rheo. Acta.* 1972;11(3):241–252.
13. Pouplin A, Masbernat O, Décarre S, Liné A. Transition to turbulence in a dispersed liquid-liquid horizontal flow. 7th International Conference on Multiphase Flow. ICMF' 2010, Tampa, FL, May 30–June 4.
14. Matas JP, Morris JF, Guazzelli E. Transition to turbulence in particulate pipe flow. *Phys. Rev. Lett.* 2003;90(1):014501
15. Pal R. Shear viscosity behavior of emulsions of two immiscible liquids. *J. Colloid Interface Sci.* 2000; 225:359–366.
16. Ovarlez G, Rodts S, Ragouilliaux A, Coussot P, Goyon J, Colin A. Wide-gap Couette flows of dense emulsions: Local concentration measurements, and comparison between macroscopic and local constitutive law measurements through magnetic resonance imaging. *Phys. Rev. E.* 2008;78:036307
17. Mason TG, Bibette J, Weitz DA. Yielding and flow of monodisperse emulsions. *J. Colloids Interface Sci.* 1996;179:439–448.
18. Bécu L, Manneville S, Colin A. Yielding and flow in adhesive and nonadhesive concentrated emulsions. *Phys. Rev. Lett.* 2006;96:138302
19. Mason TG. New fondamental concepts in emulsion rheology. *Curr. Opinion Colloid Interface Sci.* 1999;4(3):231–238
20. Goyon J, Colin A, Ovarlez G, Ajdari A, Bocquet L. Spatial cooperativity in soft glassy flows. *Nature.* 2008;454:84–87.
21. Ovarlez G, Bertrand F, Rodts S. Local determination of the constitutive law of a dense suspension of noncolloidal particles through magnetic resonance imaging. *J. Rheol.* 2006;50(3):259–292.
22. Jager-Lézer N, Tranchant JF, Alard V, Vu C, Tchoreloff PC, Grossiord JL. Rheological analysis of highly concentrated w/o emulsions. *Rheo. Acta.* 1998;37:129–138.
23. Zarraga IE, Hill DA, Leighton DT. The characterization of the total stress of concentrated suspensions of noncolloidal spheres in Newtonian fluids. *J. Rheol.* 2000;44(2):195–220.
24. Salmon JB, Bécu L, Manneville S, Colin A. Towards local rheology of emulsions under Couette flow using Dynamic Light Scattering. *Eur. Phys. J. E.* 2003;10:209–221.
25. Briceño MI, Joseph DD. Self-lubricated transport of aqueous foams in horizontal conduits. *Int. J. Multiphase Flow.* 2003;29:1817–1831.
26. Lecampion B, Garagash D. Confined flow of suspensions modeled by a frictional rheology. *J. Fluid Mech.* 2014;759:197–235.
27. Leighton DT, Acrivos A. The shear-induced migration of particles in concentrated suspensions. *J. Fluid Mech.* 1987;181:415–439.
28. Phillips RJ, Armstrong RC, Brown RA, Graham AL, Abbott JR. A constitutive model for concentrated suspensions that accounts for shear-induced particle migration. *Phys. Fluids A.* 1992;4:30–40.
29. Nott PR, Brady JF. Pressure-driven flow of suspensions: simulation and theory. *J. Fluid Mech.* 1994;275:157–199.
30. Fang Z, Mammoli A, Brady JF, Ingber MS, Mondy LA, Graham AL. Flow-aligned tensor models for suspension flows. *Int. J. Multiphase Flow.* 2002;28:137–166.
31. Lowenberg M, Hinch EJ. Numerical simulation of a concentrated emulsion in shear flow. *J. Fluid Mech.* 1996;321:395–419.
32. Zinchenko AZ, Davis RH. Shear flow of highly concentrated emulsions of deformable drops by numerical simulations. *J. Fluid Mech.* 2002;455:21–62.
33. Chan PCH, Leal LG. The motion of a deformable drop in a second order fluid. *J. Fluid Mech.* 1979;92(1):131–170.
34. Ramachandran A, Loewenberg M, Leighton DT. A constitutive equation for droplet distribution in unidirectional flows of dilute emulsions for low capillary numbers. *Phys. Fluids.* 2002;22:083301
35. Zinchenko AZ. Effect of hydrodynamic interactions between the particles on the rheological properties of dilute emulsions. *Prikl. Matem. Mekhan.* 1984;48(2):282–292.
36. Gallier S, Lemaire E, Peters F, Lobry L. Rheology of sheared suspensions of rough frictional particles. *J. Fluid Mech.* 2014;757:514–549.
37. Acrivos A, Mauri R, Fan X. Shear-induced resuspension in a couette device. *Int. J. Multiphase Flow.* 1993;19(5):797–802.